

*Journal of*

**Journal of Geophysical Research: Solid Earth**

Supporting Information for

**Anomalously high heat flow regions beneath the Transantarctic Mountains and Wilkes Subglacial Basin in East Antarctica inferred from Curie depth**

Maximilian Low<sup>e1,2</sup>, Ben Mather<sup>3</sup>, Chris Green<sup>4</sup>, Tom A. Jordan<sup>1</sup>, Jörg Ebbing<sup>5</sup>, Robert Larter<sup>1</sup>

<sup>1</sup>British Antarctic Survey, Cambridge, United Kingdom.

<sup>2</sup>The University of Edinburgh, Edinburgh, United Kingdom.

<sup>3</sup>The University of Sydney, Sydney, Australia.

<sup>4</sup>University of Leeds, Leeds, United Kingdom.

<sup>5</sup>Christian-Albrechts-Universität zu Kiel, Kiel, Germany.

**Contents of this file**

Text S1 to S13  
Figures S1 to S13

**Introduction**

This supporting information files provides information on the upward continuation of the magnetic data in S1, the effect of steps size between the windows in S2, a sensitivity test of a dry ice sheet base scenario and ice-free scenario in S3 as well as illustrates the effect of varying wavenumber range on the CDP estimation in S4.

**S1 Upward continuation**

The selected magnetic data from ADMAP-2 (Figure S1a) was upward continued using the CompuDrape extension of Geosoft. In order to perform the upward continuation of the

magnetic data an elevation grid is required containing the flight height of the magnetic measurements (Figure S2b). This elevation grid was produced by gridding the flight heights reported in the ADMAP-2 database. The magnetic data was then upward continued to a constant elevation of 4000 m, which corresponds to the highest flight altitude of the magnetic surveys.

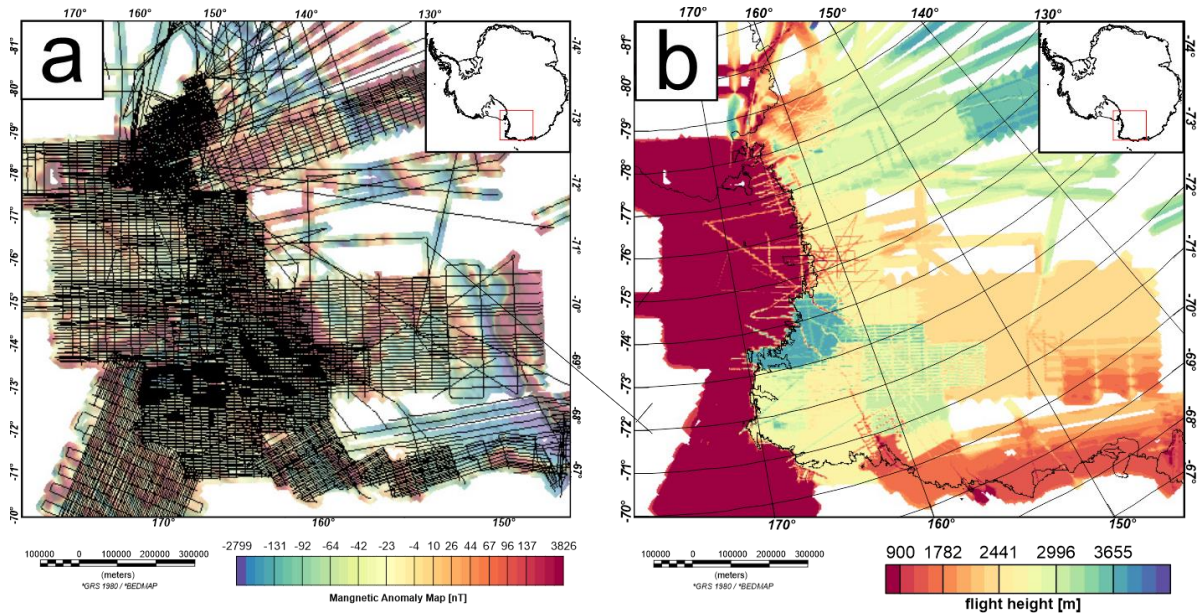


**Figure S1.** a) flight lines of selected ADMAP-2 data superimposed on ADMAP-2 magnetic data. b) flight height grid for upward continuation.

## S2 Shifting windows

The spacing between the windows in which the radially averaged power spectrum is calculated has a considerable influence on the high frequency variation within the CDP map and consequently the GHF map. A larger window spacing will result in a smoother map of CDP and GHF estimates. This effect is illustrated in Figure S2. Here, window spacing of 50 km (Figure S2a) is compared to a window spacing of 20 km (Figure S2b). Both estimates are based on a window size of 300 km. The GHF map inferred from a 50 km window spacing is considerably smoother. Nevertheless, the main GHF features are present in both maps

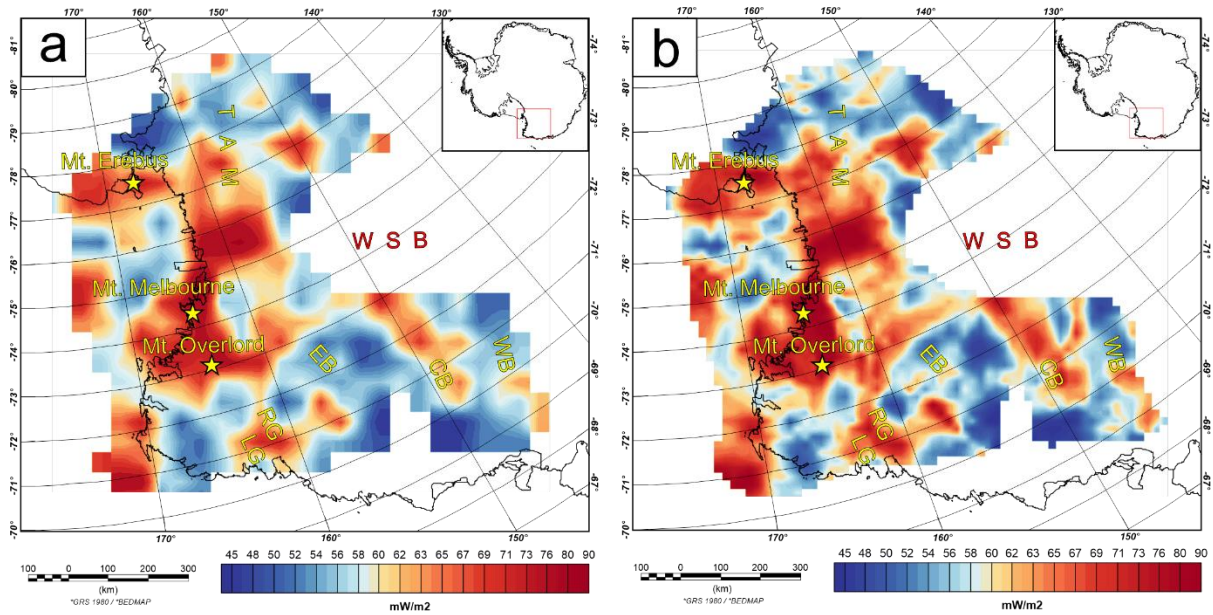


**Figure S2.** a) GHF estimates based on a window spacing of 50 km b) GHF estimates based on a window spacing of 20 km. LG, Lillie Graben; RG, Rennick Graben; EB, Eastern Basin, CB, Central Basin; WB, Western Basin; WBS, Wilkes Subglacial Basin; TAM, Transantarctic Mountains.

### S3 Dry base ice sheet and ice-free scenario

Surface temperatures are assumed to be 0 °C in equation 8. This assumption assumes a wet base of the ice sheet close to the pressure melting point of -2 °C ± a few degrees. However, temperatures are significantly lower if the base of the ice sheet is dry, or no ice cover is present. In such scenario the ice surface temperature is closer to the annual mean temperature. We performed a sensitivity test for a dry base scenario assuming a surface temperature of -30 degrees. The difference between a wet and dry base scenario is between 3 and 6 mW/m<sup>2</sup>, which is below the uncertainty of GHF inferred from Curie depth points (Figure S3).

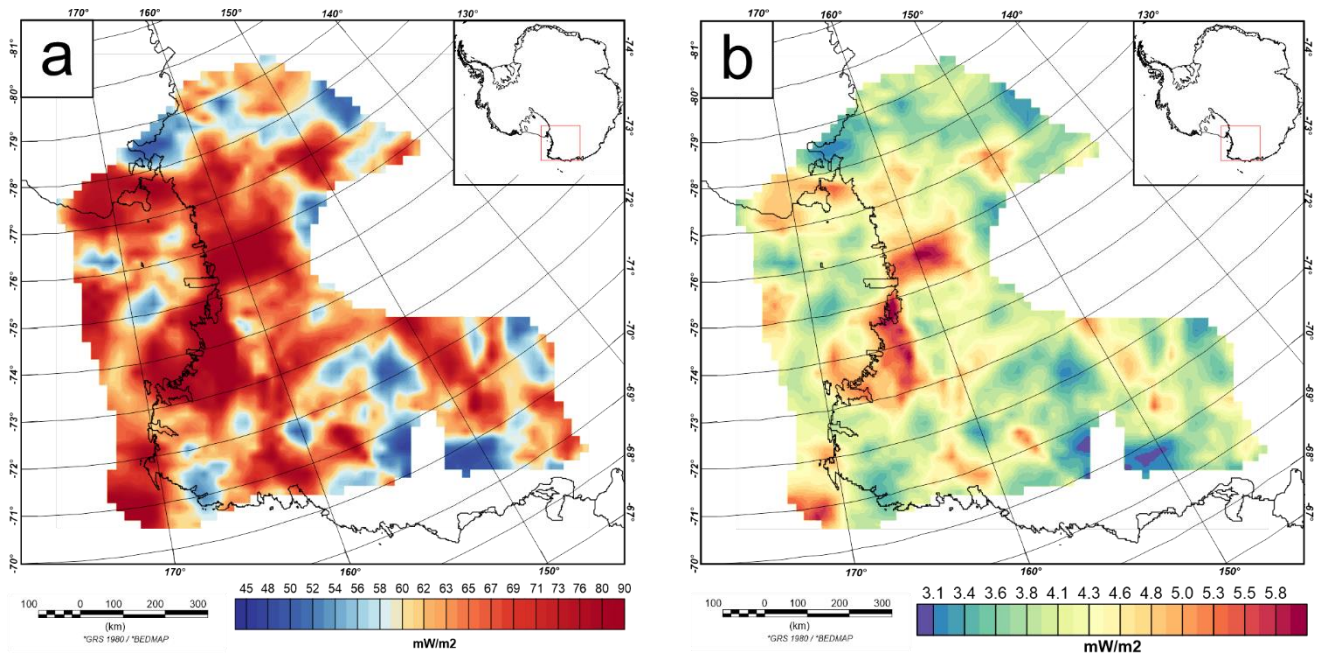


**Figure S3.** a) GHF estimates with a surface temperature of  $-30\text{ }^{\circ}\text{C}$  for an ice sheet with a dry base or ice-free scenario. b) Difference between GHF estimates using ice surface temperature of  $-30\text{ }^{\circ}\text{C}$  representing dry base of the icesheet and ice-free scenario and bedrock surface temperature of  $0\text{ }^{\circ}\text{C}$  representing an ice sheet with a wet base.

#### S4 Wavenumber variation

Selecting the correct wavenumber range to estimate  $Z_0$  and  $Z_t$  is crucial for the estimation of the bottom of magnetic source which is interpreted as the Curie depth point. Varying the low wavenumber range (long wavelength content) can change the result for  $Z_0$  by several km (Figures S4 – S13). Including or excluding one data point in the low wavenumber part of the power spectrum results in a variation of  $Z_0$  estimation of a few km (Figure S4 b-d, S8 b-d, S10 b-d, S12 b-d). Equation 6 (main manuscript) states that  $Z_0$  is multiplied by two. Therefore, the uncertainty which originates from a poorly selected wavenumber range for  $Z_0$  is magnified. The low wavenumber content between the different windows does not vary significantly in our study and hence a suitable wavenumber range for  $Z_0$  can be identified and selected by inspecting power spectra from different windows (Figures S4, S6, S8, S10, S12). The high wavenumber content differs strongly for different windows in our study (Figures S5, S7, S9, S11, S13). However, the influence of different wavenumber ranges has only a little effect on the  $Z_t$  estimation (Figures S5 b-d, S7 b-d, S9 b-d, S11 b-d, S13 b-d). Including or excluding a

large portion of data points to estimate  $Z_t$  results only in a variation of roughly 300 meters (Figure 12 b-d). In contrast to  $Z_0$  the  $Z_t$  value is not multiplied in equation 6 and is therefore overall, less dominant than the  $Z_0$  value to estimate the CDP. Using a constant wavenumber range for all windows in an automated process is robust because i) the low wavenumber range to estimate  $Z_0$  is very stable, and a suitable wavenumber range can be selected and ii) the strong variation in the high wavenumber range is negligible since choosing a wrong wavenumber range (Figures S5, S7, S9, S11, S13) results in a variation of the CDP below the formal uncertainty. In other words, the method is not sensitive to variation in a sub km scale.

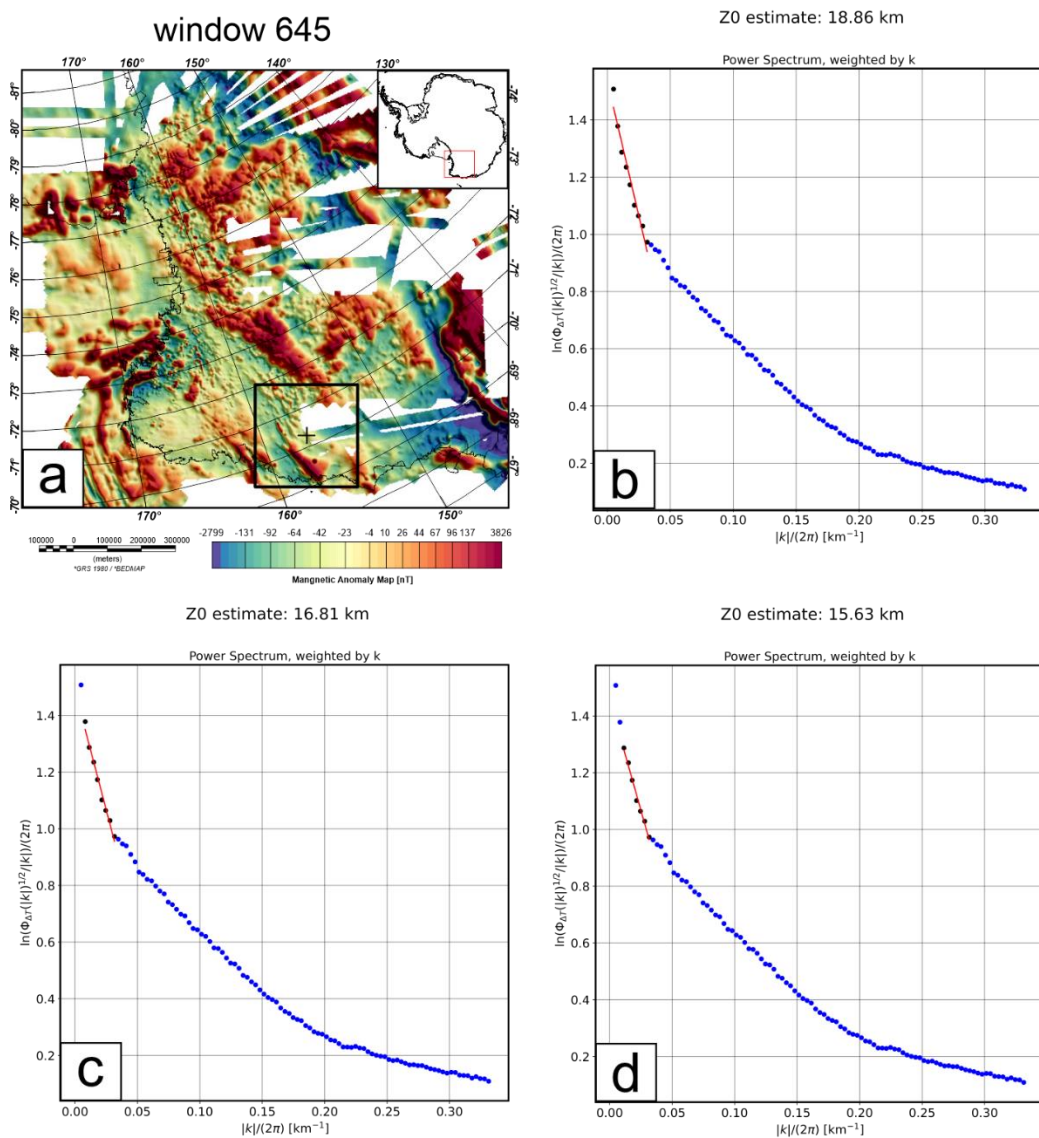


**Figure S4.** a) Power spectrum from window 645 with a window size of 300 km. Blue dots power spectrum data points. Black dots indicate data points used for the linear regression. Red line

linear fit to estimate  $Z_0$  a) Window location and extent superimposed on magnetic data. b) wavenumber range  $0 - 0.033 |k|/2\pi$ ,  $Z_0$  estimate: 18.86 km. c) wavenumber range  $0.006 - 0.033 |k|/2\pi$ ,  $Z_0$  estimate: 16.91 km. d) wavenumber range  $0.01 - 0.033 |k|/2\pi$ ,  $Z_0$  estimate: 15.63 km.

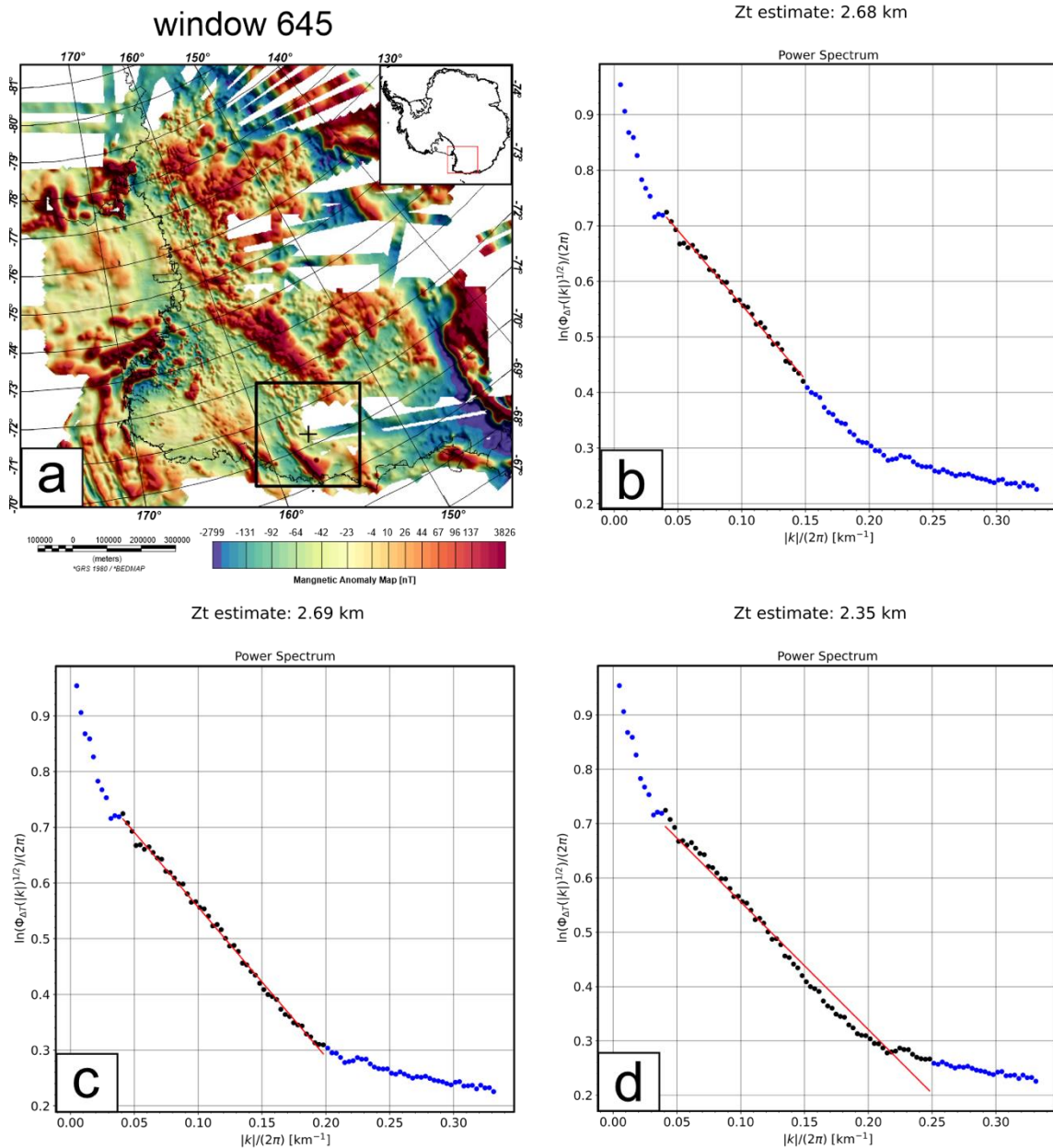


**Figure S5.** Power spectrum from window 645 with a window size of 300 km. Blue dots power spectrum data points. Black dots indicate data points used for the linear regression. Red line linear fit to estimate  $Z_0$ . a) Window location and extent superimposed on magnetic data. b)

wavenumber range  $0.04 - 0.25 \ |k|/2\pi$ ,  $Z_t$  estimate: 2.68 km. c) wavenumber range  $0.04 - 0.2 \ |k|/2\pi$ ,  $Z_t$  estimate: 2.69 km d) wavenumber range  $0.04 - 0.15 \ |k|/2\pi$ ,  $Z_t$  estimate: 2.35 km.

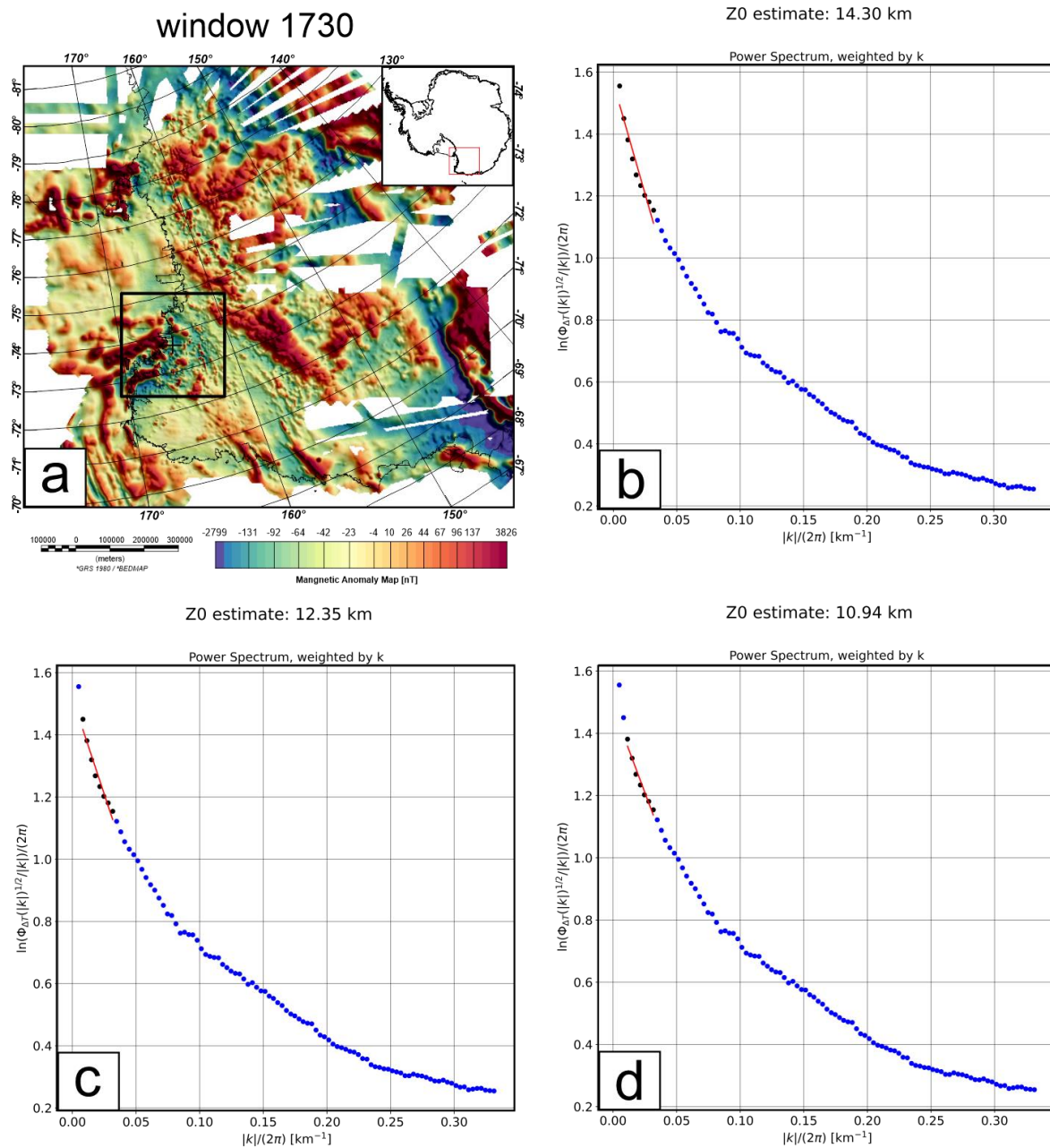
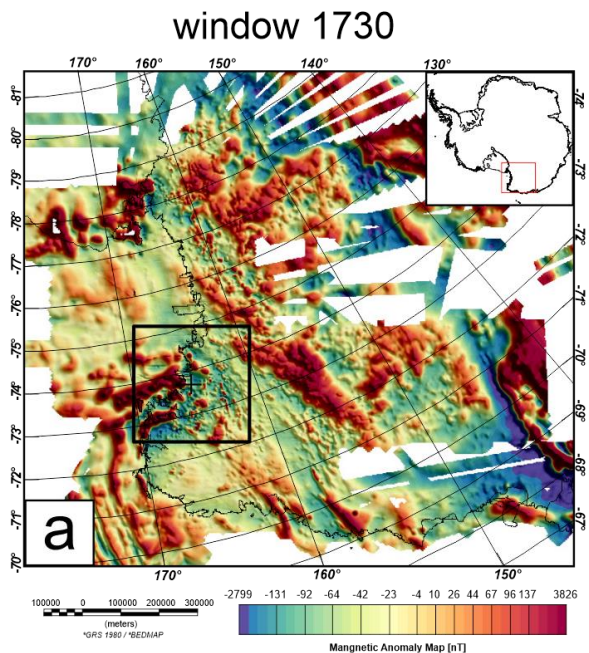
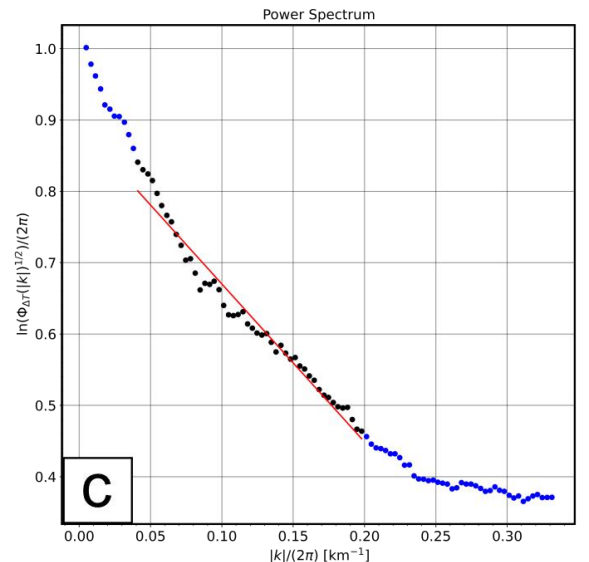


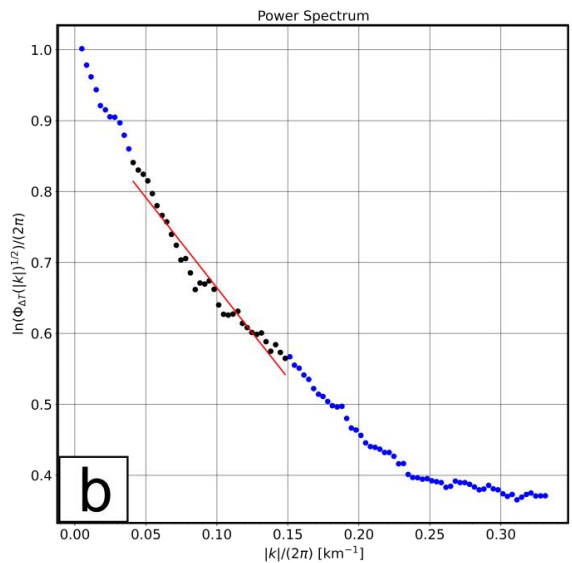
**Figure S6.** Power spectrum from window 1730 with a window size of 300 km. Blue dots power spectrum data points. Black dots indicate data points used for the linear regression. Red line linear fit to estimate  $Z_0$  a) Window location and extent superimposed on magnetic data. b) wavenumber range  $0 - 0.033 \ |k|/2\pi$ ,  $Z_0$  estimate: 14.3 km. c) wavenumber range wavenumber range  $0.006 - 0.033 \ |k|/2\pi$ ,  $Z_0$  estimate: 12.35 km. d) wavenumber range  $0.01 - 0.033 \ |k|/2\pi$ ,  $Z_0$  estimate: 10.94 km.



Zt estimate: 2.21 km



Zt estimate: 2.54 km



Zt estimate: 2.06 km

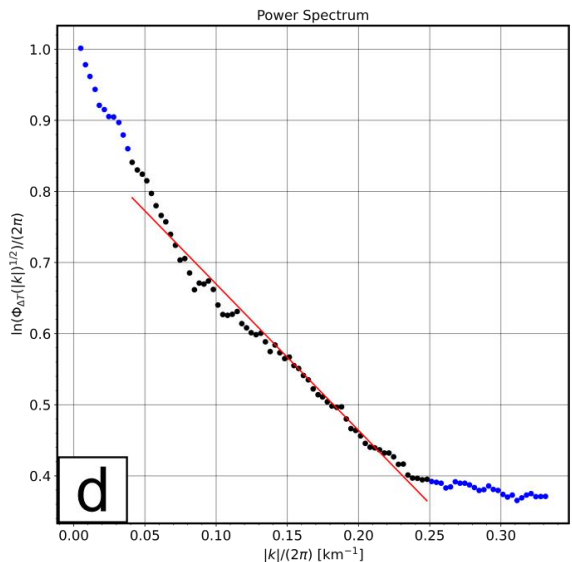


**Figure S7.** Power spectrum from window 645 with a window size of 300 km. Blue dots power spectrum data points. Black dots indicate data points used for the linear regression. Red line linear fit to estimate Z0. a) Window location and extent superimposed on magnetic data. b)

wavenumber range  $0.04 - 0.25 \ |k|/2\pi$ ,  $Z_t$  estimate: 2.54 km. c) wavenumber range  $0.04 - 0.2 \ |k|/2\pi$ ,  $Z_t$  estimate: 2.21 km. d) wavenumber range  $0.04 - 0.15 \ |k|/2\pi$ ,  $Z_t$  estimate: 2.06 km.

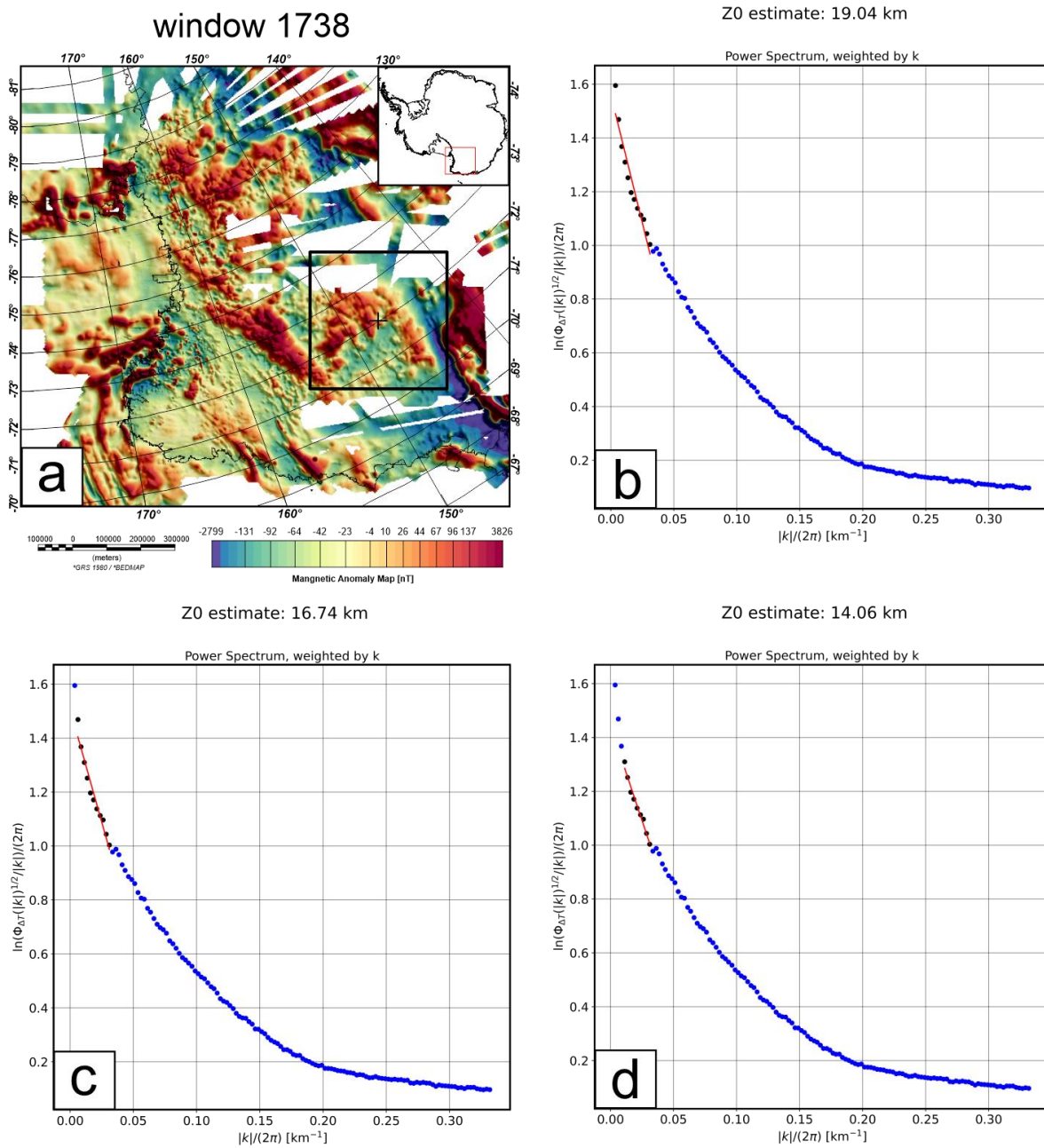


**Figure S8.** Power spectrum from window 1730 with a window size of 400 km. Blue dots power spectrum data points. Black dots indicate data points used for the linear regression. Red line linear fit to estimate  $Z_0$  a) Window location and extent superimposed on magnetic data. b) wavenumber range  $0 - 0.033 \ |k|/2\pi$ ,  $Z_0$  estimate: 19.04 km. c) wavenumber range wavenumber

range 0.006 – 0.033  $|k|/2\pi$ , Z0 estimate: 16.74 km. d) wavenumber range 0.01 – 0.033  $|k|/2\pi$ , Z0 estimate: 14.06 km.

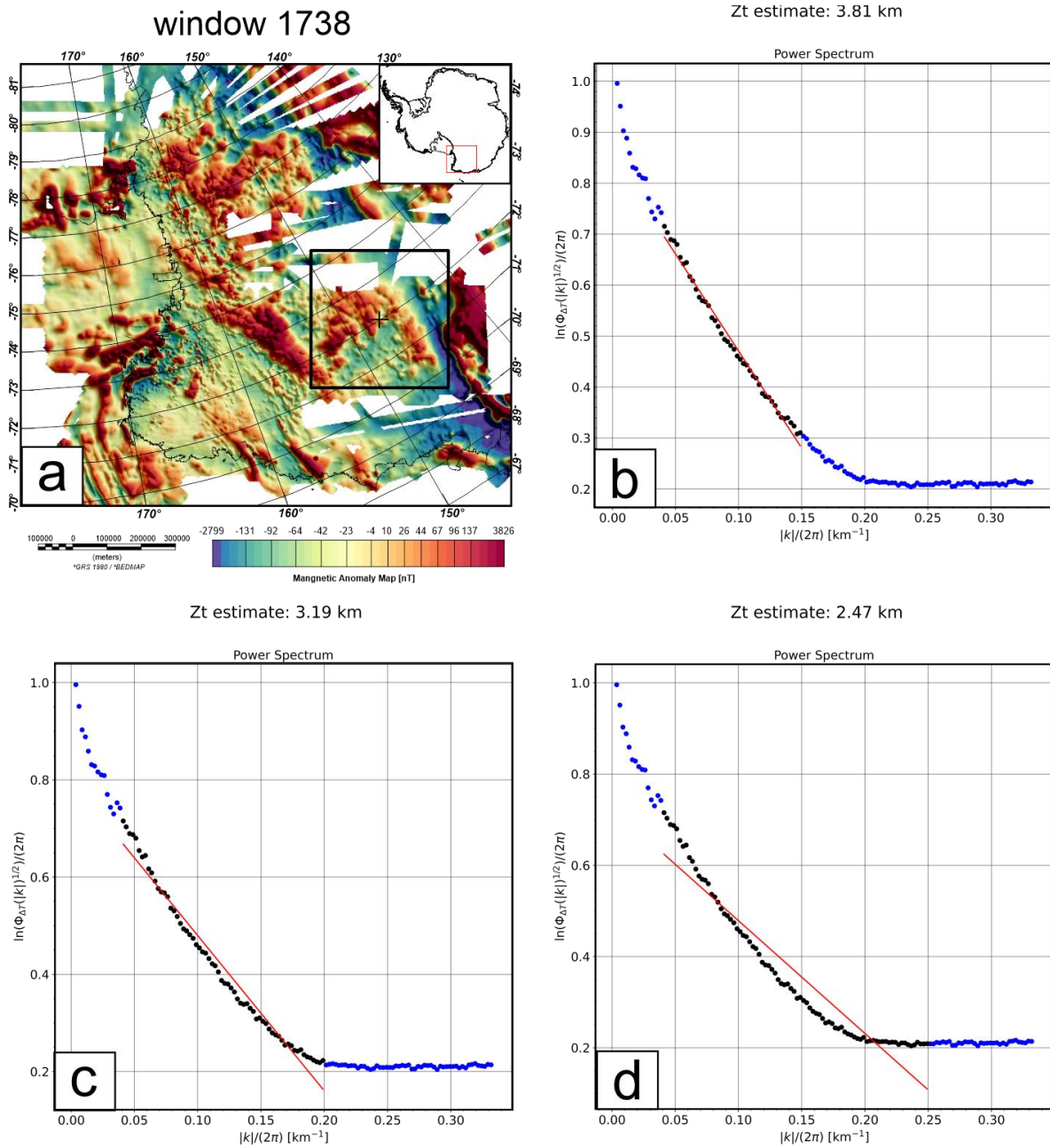
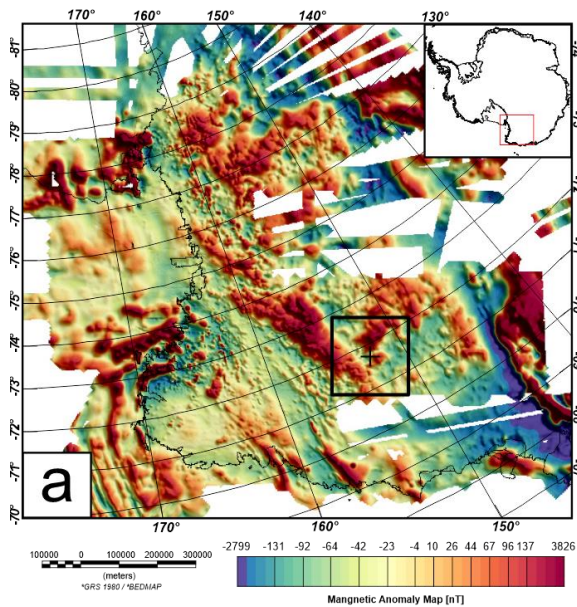


**Figure S9.** Power spectrum from window 1738 with a window size of 400 km. Blue dots power spectrum data points. Black dots indicate data points used for the linear regression. Red line linear fit to estimate Z0. a) Window location and extent superimposed on magnetic data. b)

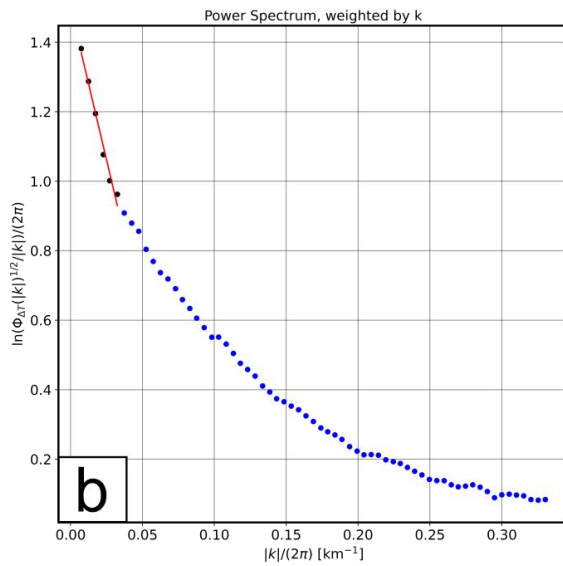
wavenumber range 0.04 – 0.25  $|k|/2\pi$ , Zt estimate: 3.81 km. c) wavenumber range 0.04 – 0.2  $|k|/2\pi$ , Zt estimate: 3.19 km d) wavenumber range 0.04 – 0.15  $|k|/2\pi$ , Zt estimate: 2.47 km.

window 1856

Z0 estimate: 17.52 km



Z0 estimate: 16.80 km



Z0 estimate: 15.34 km

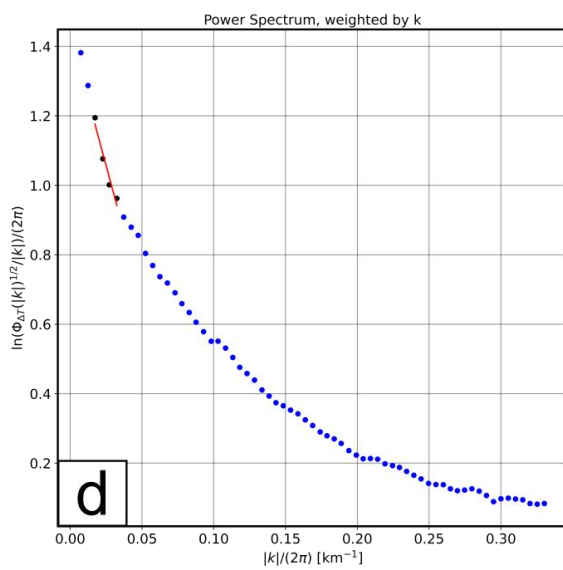
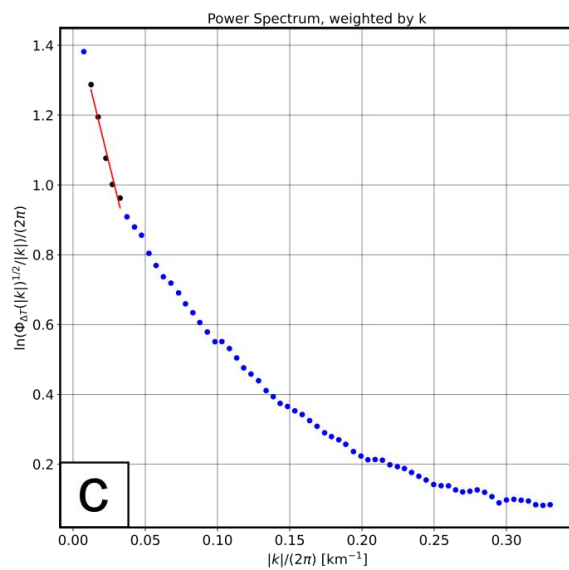


**Figure S10.** Power spectrum from window 1730 with a window size of 200 km. Blue dots power spectrum data points. Black dots indicate data points used for the linear regression. Red line linear fit to estimate Z0 a) Window location and extent superimposed on magnetic data. b) wavenumber range 0 – 0.033  $|k|/2\pi$ , Z0 estimate: 17.52 km. c) wavenumber range wavenumber

range 0.01 – 0.033  $|k|/2\pi$ ,  $Z_0$  estimate: 16.8 km. d) wavenumber range 0.015 – 0.033  $|k|/2\pi$ ,  $Z_0$  estimate: 15.34 km.

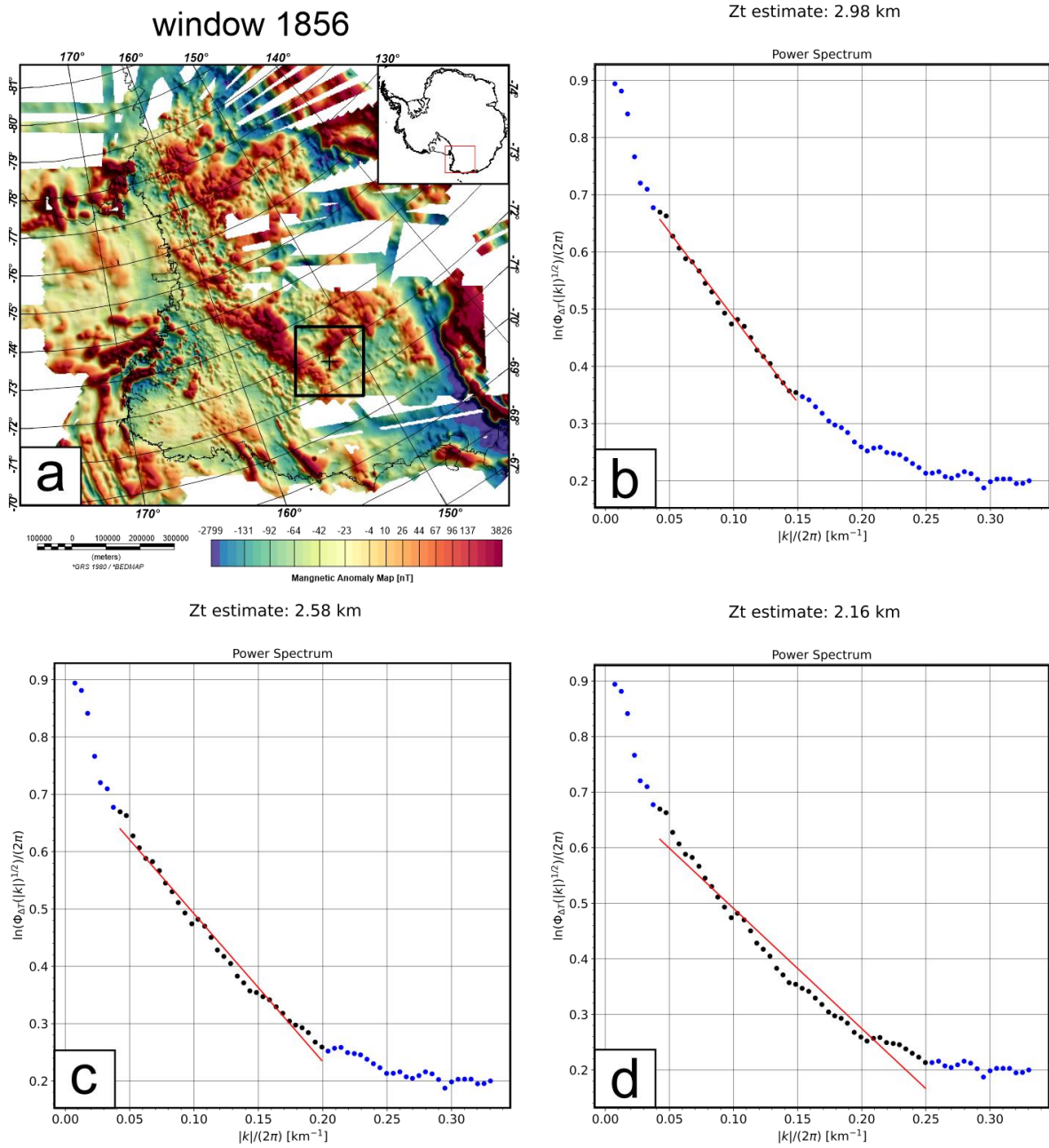


**Figure S11.** Power spectrum from window 1738 with a window size of 200 km. Blue dots power spectrum data points. Black dots indicate data points used for the linear regression. Red line linear fit to estimate  $Z_0$ . a) Window location and extent superimposed on magnetic data. b) wavenumber range 0.04 – 0.25  $|k|/2\pi$ ,  $Z_t$  estimate: 2.98 km. c) wavenumber range

0.04 – 0.2  $|k|/2\pi$ ,  $Z_t$  estimate: 2.58km d) wavenumber range 0.04 – 0.15  $|k|/2\pi$ ,  $Z_t$  estimate: 2.16 km.

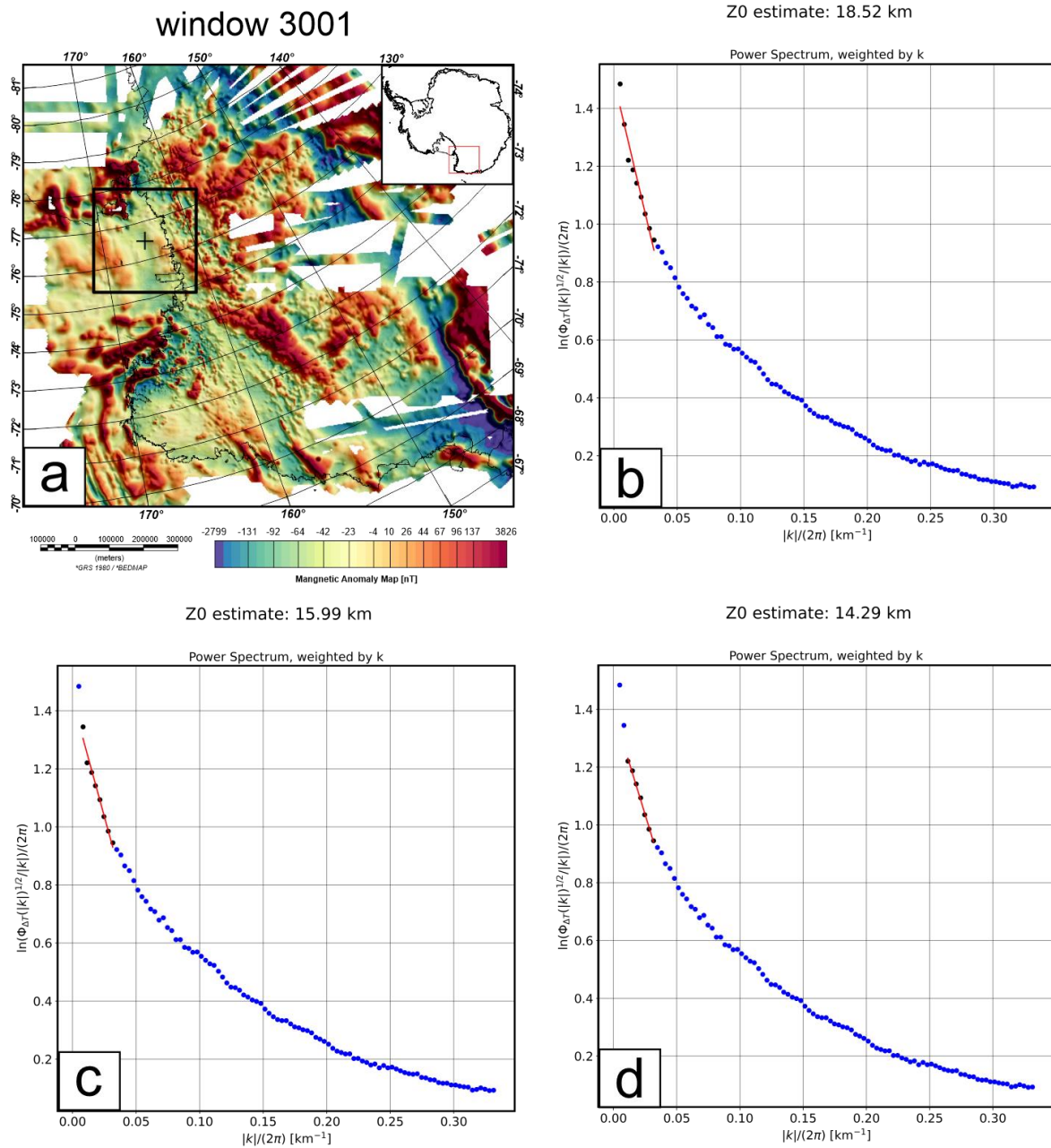


**Figure S12.** Power spectrum from window 3001 with a window size of 300 km. Blue dots power spectrum data points. Black dots indicate data points used for the linear regression. Red line linear fit to estimate  $Z_0$  a) Window location and extent superimposed on magnetic data. b) wavenumber range 0 – 0.033  $|k|/2\pi$ ,  $Z_0$  estimate: 18.52 km. c) wavenumber range

wavenumber range  $0.006 - 0.033 \text{ } |k|/2\pi$ , Z0 estimate: 15.99 km. d) wavenumber range  $0.01 - 0.033 \text{ } |k|/2\pi$ , Z0 estimate: 14.29 km.

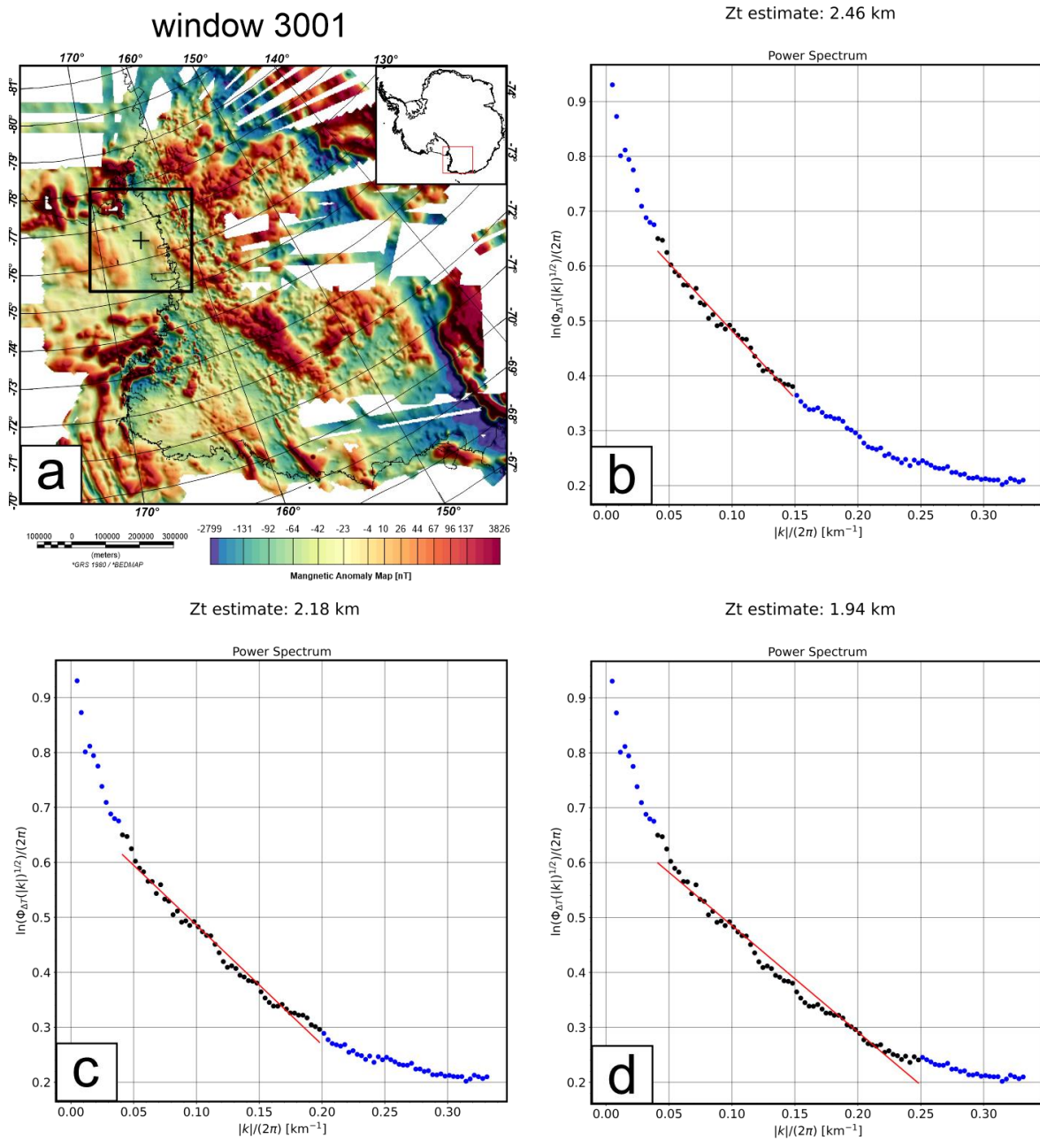


**Figure S13.** Power spectrum from window 1738 with a window size of 300 km. Blue dots power spectrum data points. Black dots indicate data points used for the linear regression. Red line linear fit to estimate Z0. a) Window location and extent superimposed on magnetic data. b) wavenumber range  $0.04 - 0.25 \text{ } |k|/2\pi$ , Zt estimate: 2.46 km. c) wavenumber range  $0.04 - 0.2 \text{ } |k|/2\pi$ , Zt estimate: 2.18 km d) wavenumber range  $0.04 - 0.15 \text{ } |k|/2\pi$ , Zt estimate: 1.94 km.